

ALGORITHMIC ELABORATION ON MULTI-SOURCE IMAGE REGISTRATION IN REMOTE SENSING

Joz Wua, *, Ming-Che Liub, Chi Changc

^a Prof., Ctr. for Space and Remote Sensing Res., NCU., Jhongli 320, Taiwan, CHINA. – jozwu@csrsr.ncu.edu.tw

^b Graduated student, Dept. of Civil Engrg., NCU, Jhongli 320, Taiwan, CHINA. – 953202067@cc.ncu.edu.tw

^c PH. D. candidate, Dept. of Civil Engrg., NCU, Jhongli 320, Taiwan, CHINA. – elsacduck@yahoo.com.tw

Commission VII, WG VII/5

KEY WORDS: Image Processing, Image Matching, Digital Photogrammetry, Multi-source, Image Registration

ABSTRACT:

When performing an image-based change detection, it is necessary to make sure that two comparing remote-sensing images have been well co-registered. An analyst can check if the two images are both ortho-rectified. Or he can refine the between-image registration, skipping the process of geo-coding the images once more. The objective of the paper is to deal with image-to-image registration, especially for multi-source remote sensing images that may crassly differ in radiometry and geometry. An approach that combines feature-based matching with area-based matching for automatically registering two different images is proposed. Firstly, large-scale edge gradient contours are detected by using the Canny algorithm and petty contours are cleaned by a bounding-box. Furthermore, the initial matching points are selected using a cost function that measures the gradient orientation and distance between all possible pairs of the points. Pairing image windows are built and segmented to get radiometric parameters, and the radiometric parameters are used here to modulate the slave image window. Finally, master image window and modulated slave image window are matched by least-squares matching, and control points are found. The thin-plate splines method is used to register master and slave images. Experimental results show that numerous matching points can be obtained correctly and automatically, and two images can be registered precisely.

1. INTRODUCTION

Image registration is the process that establishes a geometric mapping function between two different images. In order to analyze and apply remote sensing images completely, image registration is the fundamental and a key issue in remote sensing. These applications are various, such as multi-sensor image fusion, change detection, image mosaicking, motion detection and object recognition (Dai, 1999).

The automatic image registration techniques fall into two general categories: area-based and feature-based methods (Zitova and Flusser, 2003). Area-based methods are the classical method which uses the gray value of the pixels to describe matching relation. A small window of pixels in the slave image is compared statistically with windows of the same size as the master image. Feature-based methods do not use the gray value of pixels to describe matching relation, but use features, like corners, lines and regions, obtained by feature extraction algorithms from each image. In general, feature-based methods handle large misalignments with relatively short execution times, and area-based methods advance the registration accuracy to sub-pixel range (Chen *et al.*, 2007).

The purpose of this paper is to present a registration algorithm which combines feature-based matching with area-based matching approaches. It also displays the qualitative and quantitative results of this algorithm by using a SPOT 5 panchromatic image and a LIDAR-airborne amplitude image. The advantage of this algorithm is accurate, reliable and nearly automatic.

2. METHODOLOGY

The proposed image registration algorithm contains four steps: (1) manual alignment; (2) feature-based matching; (3) area-based matching; (4) coordinate transformation. Figure 1 shows the main flowchart.

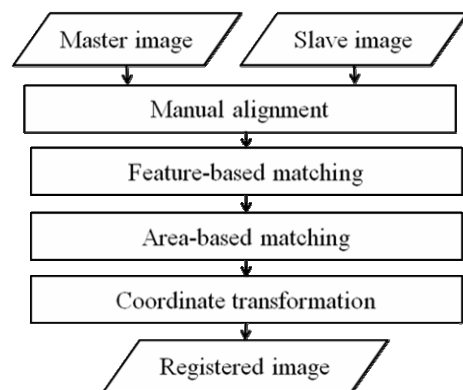


Figure 1. Flowchart of the image registration algorithm

2.1 Manual Alignment

At first, the slave image is roughly registered with the master image by using three or four manually selected tie points. This step can remove rotation and scale errors and reduce shift errors within a few pixels in two images.

Since the efficiency of the after procedure can be enhanced by the manual alignment, it is necessary in this research even though it is not automatic. Moreover, it provides the user to

ensure that the overlap and coverage of the area is adequate enough (Dare and Downman, 2001).

2.2 Feature-Based Matching

The aim of feature-based matching is to extract the line features and find the initial matching point pairs. In this paper, the algorithm of Hong and Schowengerdt (2005) is used. Figure 2 shows the feature-based matching flowchart.

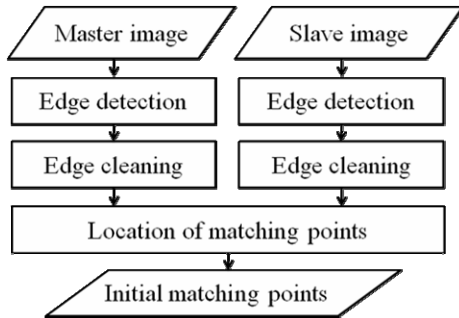


Figure 2. Flowchart of the feature-based matching process

2.3.1 Edge Detection

An optimal edge detector needs to conform to the following criteria:

1. Good detection: The algorithm should detect real edges in the image as many as possible, and it should not mark error edges.
2. Good localization: The distance between the position of the detected and real edge in the image should be as close as possible.
3. Minimal response: An edge in the image should be detected once.

Canny algorithm (Canny, 1986) is the most general method for edge detected and its advantage includes all of above. The processes of Canny algorithm are:

1. Noise reduction: At first, the image is convolved by a Gaussian filter with a scale σ so as to reduce the effect of the noises. The function of Gaussian filter is written as:

$$G(x, y, \sigma) = \frac{1}{2\pi\sigma^2} e^{-(x^2+y^2)/2\sigma^2} \quad (1)$$

Finding the intensity gradient of the image: The gradient orientation, $\theta(x, y)$, and magnitude, $m(x, y)$, of the edge can be determined by:

$$\theta(x, y) = \tan^{-1} \left(\frac{\partial f_g / \partial y}{\partial f_g / \partial x} \right) \quad (2)$$

$$m(x, y) = \sqrt{\left(\frac{\partial f_g}{\partial x} \right)^2 + \left(\frac{\partial f_g}{\partial y} \right)^2}$$

where $\partial f_g / \partial x$ and $\partial f_g / \partial y$ can be defined by Roberts, Sobel or other edge detection operators. The edge orientation is

integrated with four angles representing vertical, horizontal and the two diagonals.

2. Non-maximum suppression: If the gradient magnitude of each pixel is not the greatest among the neighboring edge pixels of gradient orientation, the pixel is sure not the edge.

3. Hysteresis threshold: Edge detection in the image with the hysteresis threshold step is to eliminate spurious responses. The step needs to set two threshold t_0, t_1 and t_0 is less than t_1 . If the gradient magnitude of every pixel which survives last process is greater than t_1 , it is true edges. On the contrary, if it is less than t_0 , it is false edges. All remaining pixels within t_0 and t_1 are inspected. If one or more than one neighboring pixels of the inspected pixel are already true edges, the inspected pixel is also the true edges. The step for check may be repeated until no pixels become true edges.

2.3.2 Edge Cleaning

This step is designed to eliminate petty edges in the edge image. Two types of edges are considered petty edges. One is an edge which is shorter than a threshold value and another is a long edge which contains a small area only (Hong and Schowengerdt, 2005).

A method to detect short edge is to use bounding box. If the bounding box size of an edge is less than the setting threshold, the edge is defined as a petty edge and deletes it. The method can reduce the error rate of later matching process.

2.3.3 Location of matching points

The edge matching process is based on the algorithm by Newton *et al.* (1994). Figure 3 shows how to match the points of edges from slave image to master image.

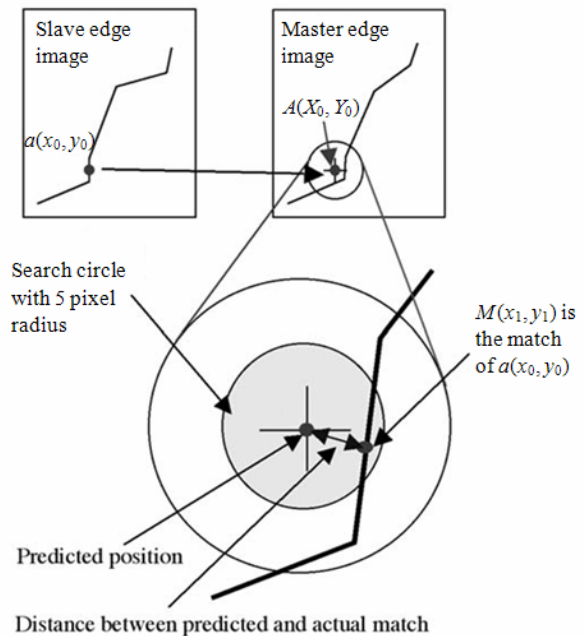


Figure 3. Matching points between two images (Hong and Schowengerdt, 2005)

$A(X_0, Y_0)$ is the predicted point in the master image. By utilizing the manual-registered transform function, $A(X_0, Y_0)$ can be transformed into $a(x_0, y_0)$ in the slave image. And then, a circle with a radius of 5 pixels is defined. All pixels of edges within

the circle are considered as possible matching points. A cost function which includes gradient orientation and distance between predicted and actual position is determined by (Hong and Schowengerdt, 2005):

$$C = \alpha \times d + \beta \times |\theta_{\text{Master}} - \theta_{\text{Slave}}| \quad (3)$$

where α : 1 over maximum tolerance distance (pixels⁻¹)
 β : 1 over maximum tolerance orientation (radians⁻¹)
 d : distance between predicted and actual match (pixels)
 θ_{Master} : the gradient orientation of master point of edge (radians)
 θ_{Slave} : the gradient orientation of slave point of edge (radians)

The point of edge whose cost function is a minimum is the initial matching point.

2.3 Area-Based Matching

Figure 4 shows the area-based matching flowchart. Area-based matching methods usually apply the same or similar spectral images in the experience. If the difference between the spectrum of master image and the spectrum of slave image is large, it is necessary to use feature-based matching methods. Therefore, the radiometric parameters of the two multi-spectral images should be adjusted in order to match by using area-based matching methods.

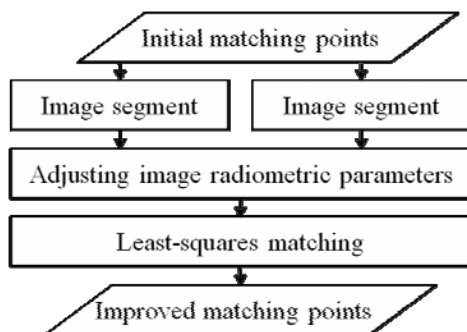


Figure 4. Flowchart of the area-based matching process

2.3.1 Image segment

Before adjusting image radiometric parameters, each initial matching point pair is needed to build a window and this window is segmented by the between-class variance method (Tsai, 1995). At first, the probability of gray value in a window opened by each initial matching point is defined by:

$$p_i = I(i) / \sum_{i=0}^{255} I(i); i \in \{0, 1, K, 255\} \quad (4)$$

where $I(i)$ is the estimation of gray value in the window. And then, the parameters of the optimal standard function can be computed as follows:

$$w_0 = \sum p_i, m_0 = \frac{1}{w_0} \sum ip_i; 0 \leq i \leq T \quad (5)$$

$$w_1 = \sum p_i, m_1 = \frac{1}{w_1} \sum ip_i; T < i \leq 255$$

The optimal standard function is defined by:

$$V(T) = w_0 w_1 (m_1 - m_0)^2 \quad (6)$$

When $V(T)$ is maximum, T is the threshold of image segment. The result of image segment is shown as the figure 5.

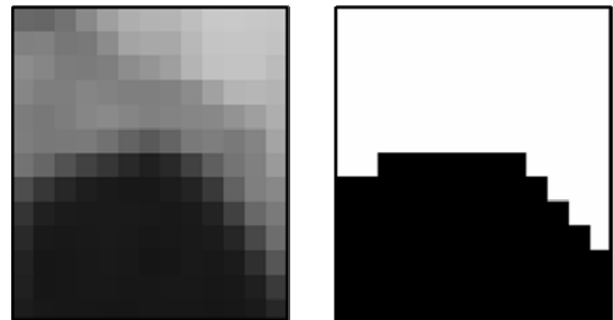


Figure 5. Image segment

2.3.2 Adjusting image radiometric parameters

The histogram equalization method can be conducted after the process of image segment, and the gray value model is defined by:

$$G_s = h_1 + h_2 G_M \quad \text{or} \quad G_M = \frac{(G_s - h_1)}{h_2} \quad (7)$$

where G_s refers the gray value of a slave pixel, G_M refers a corresponding master pixel value, h_1 stands for a gray value shift, and h_2 stands a linear scale parameter. The parameters h_1 and h_2 are defined as:

$$H_1 = \mu_s - \frac{\sigma_s}{\sigma_M} \mu_M \quad (8)$$

$$H_2 = \frac{\sigma_s}{\sigma_M}$$

where (μ_s, σ_s) and (μ_M, σ_M) are the segment-based gray-level means and standard deviations, respectively.

2.3.3 Least-squares matching

A least-squares image matching method yields an optimal position in this process, where the sum of squares of the post-fit residuals of the gray value becomes a minimum.

By supposing the gray value of a slave-pixel error, $v_s \sim N(0, \sigma_s^2)$, and a master-pixel error, $v_M \sim N(0, \sigma_M^2)$, the

image-matching functional model is defined for:

$$G_M(X, Y) = h_1 + h_2 G_S \left(\begin{bmatrix} a_1 & a_2 & a_3 \\ b_1 & b_2 & b_3 \end{bmatrix} \begin{bmatrix} 1 \\ X \\ Y \end{bmatrix} \right) \quad (9)$$

$$= h_1 + h_2 G_S(X, Y; A)$$

where the coordinates (X, Y) and the affinity parameters $(a_1, a_2, a_3, b_1, b_2, b_3)$ are included. If a bar is used for parametric approximation, equation 9 can be linearized by Taylor's expansion. The result of the terms is:

$$v_S - \bar{h}_2 v_M - dh_1 - \bar{G}_M dh_2 - \bar{h}_2 \bar{G}_{Mx} (da_1 + xda_2 + yda_3) - \bar{h}_2 \bar{G}_{My} (db_1 + xdb_2 + ydb_3) = -G_S + \bar{h}_1 + \bar{h}_2 \bar{G}_M \quad (10)$$

where \bar{G}_{Mx} stands for the gradient of the gray value in the line direction, and \bar{G}_{My} represents the gradient in the sample direction. We can formulate a matrix equation based on equation 10 as:

$$\mathbf{Bv} + \mathbf{Ax} = \mathbf{l} \quad (11)$$

where $\mathbf{B}_{a \times 2a}$: the coefficient matrix

$$\mathbf{v}_{2a \times 1} = (v_{S1}, v_{M1}, v_{S2}, v_{M2}, \dots, v_{Sa}, v_{Ma})^T$$

$\mathbf{A}_{n \times a}$: the design matrix

$$\mathbf{x} = (dh_1, dh_2, da_1, da_2, da_3, db_1, db_2, db_3)^T$$

$$\mathbf{l}_{a \times 1} = (\mathbf{K}, -G_{Ti} + \bar{h}_1 + \bar{h}_2 \bar{G}_{Si}, \mathbf{K})^T$$

Matrix \mathbf{x} can be obtained by the least-squares method and the necessary iteration comes to an end when the components of matrix \mathbf{x} converge. Some initial matching pairs are eliminated by area-based matching. Furthermore, the remaining matching pairs turn into the improved matching points and improve the positioning accuracy.

2.4 Coordinate Transformation

In dealing with the image for a flat area, the most common method is the affine transformation, but it is not appropriate for data with nonlinear and local geometric distortions. Thin-plate splines are one of the most widely used transformation functions in the registration of images with nonlinear geometric differences (Bentoutou *et al.*, 2005; Goshtasby, 1988).

The thin-plate splines function can be written as:

$$\mathbf{h}(\mathbf{x}) = \mathbf{Ax} + \mathbf{t} + \sum_{i=1}^m \mathbf{W}_i K(\|\mathbf{x} - \mathbf{x}_i\|) \quad (12)$$

where \mathbf{A}, \mathbf{t} : the affine transformation parameter matrices
 \mathbf{W}_i : the weights of the nonlinear radial interpolation function K
 \mathbf{x}_i : the matched points

$$K(\lambda): \text{ Biharmonic equation, } K(\lambda) = \lambda^2 \log(\lambda^2)$$

First, the estimation of the affine transformation parameters \mathbf{A} and \mathbf{t} is calculated by all improved matching points in master image, (X, Y) , and points in slave image, (x, y) . The least-squares method is used here in this procedure:

$$\mathbf{Y} = \mathbf{Mz} + \mathbf{v} \Rightarrow \mathbf{z} = (\mathbf{M}^T \mathbf{M})^{-1} (\mathbf{M}^T \mathbf{Y}) \quad (13)$$

where $\mathbf{Y}_{2n \times 1} = (X_1, Y_1, X_2, Y_2, \dots, X_n, Y_n)^T$

$\mathbf{M}_{n \times 8}$: the design matrix

$$\mathbf{z} = (a_1, a_2, a_3, b_1, b_2, b_3)^T$$

And then, each matched point pair that produces a larger error than the threshold is removed by:

$$\sqrt{(\hat{x}_i - X_i)^2 + (\hat{y}_i - Y_i)^2} < E_r \quad (14)$$

where (\hat{x}, \hat{y}) : points in slave image after affine transformation
 E_r : Threshold

At last, the remaining matching points are used to calculate the weights by:

$$\begin{bmatrix} X_1 - a_1 x_1 - a_2 y_1 - a_3 \\ X_2 - a_1 x_2 - a_2 y_2 - a_3 \\ \dots \\ X_m - a_1 x_m - a_2 y_m - a_3 \end{bmatrix} = \begin{bmatrix} 0 & K(\lambda_{12}) & \Lambda & K(\lambda_{1m}) \\ K(\lambda_{21}) & 0 & \Lambda & K(\lambda_{2m}) \\ \dots \\ K(\lambda_{m1}) & K(\lambda_{m2}) & \Lambda & 0 \end{bmatrix} \begin{bmatrix} W_{x1} \\ W_{x2} \\ \dots \\ W_{xm} \end{bmatrix} \quad (15)$$

$$\begin{bmatrix} Y_1 - b_1 x_1 - b_2 y_1 - b_3 \\ Y_2 - b_1 x_2 - b_2 y_2 - b_3 \\ \dots \\ Y_m - b_1 x_m - b_2 y_m - b_3 \end{bmatrix} = \begin{bmatrix} 0 & K(\lambda_{12}) & \Lambda & K(\lambda_{1m}) \\ K(\lambda_{21}) & 0 & \Lambda & K(\lambda_{2m}) \\ \dots \\ K(\lambda_{m1}) & K(\lambda_{m2}) & \Lambda & 0 \end{bmatrix} \begin{bmatrix} W_{y1} \\ W_{y2} \\ \dots \\ W_{ym} \end{bmatrix}$$

3. EXPERIMENTAL RESULTS

In the experiment, the master image is a LIDAR local mapping mission (2.0-m spatial resolution), was flown on June 7, 2005. The LiDAR amplitude image of a part of the Hsinchu airfield roughly one square kilometer, is shown in Figure 6a. Figure 6b displays a SPOT-5 1A panchromatic image with 2.5-m resolution acquired on April 6, 2005. The image size is 600 × 600 pixels.

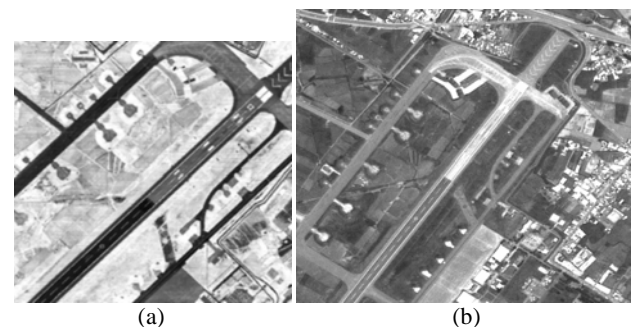
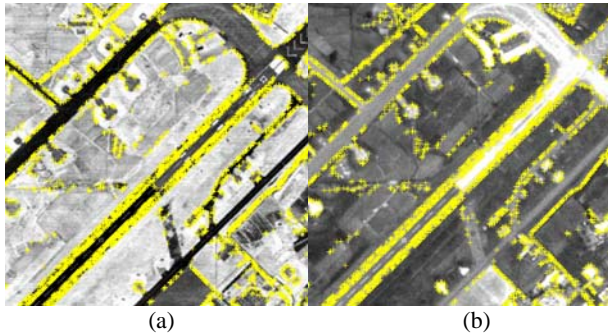


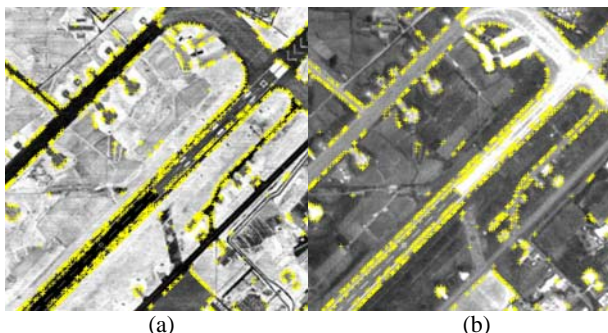
Figure 6. The master and slave image

Three or four tie points are selected manually at first, and initial matching points are obtained by the feature-based matching method. The distributions of initial matching points in master and slave image are shown in figure 7(a) and 7(b).



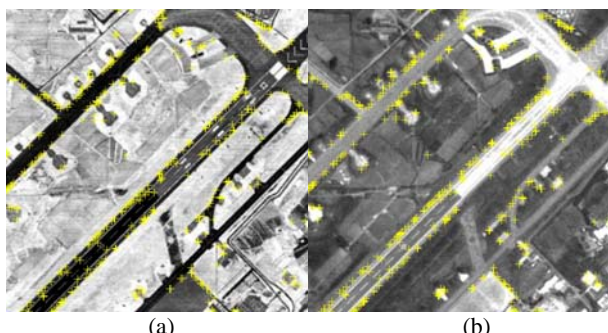
(a) (b)
Figure 7. Initial matching points

Furthermore, figure 8(a) and 8(b) shows the distributions of improved matching points are acquired from the area-based matching method.



(a) (b)
Figure 8. Improved matching points

At last, the affine transformation parameters are computed from all improved matching points and outlier-points are deleted whose errors are larger than 1 pixels. The distributions of remaining matching points are shown in figure 9(a) and 9(b). The inter-tile image after image registration by the Thin-plate splines method is shown in figure 10.



(a) (b)
Figure 9. Remaining matching points

Table 1 presents the comparisons between points are only extracted from the feature-based matching method and the feature- plus area-based matching method. In this table, ten check points are selected manually. Table 1 indicates that unit weight standard deviation and RMSE computed by the feature-

plus area-based matching method are better than the feature-based matching method.

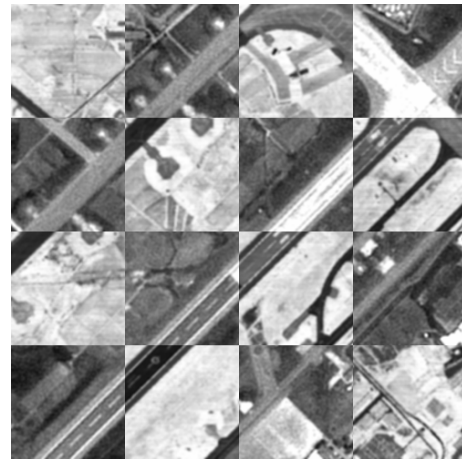


Figure 10. Inter-tile image

Dataset	Feature-based	Feature- plus area-based
Number of matched points before deleting outliers	3649	1716
Unit weight standard deviation of matched points before deleting outliers (pixels)	2.53	2.16
RMSE before deleting outliers (pixels)	2.17	1.95.
Number of matched points after deleting outliers	497	401
Unit weight standard deviation of matched points after deleting outliers (pixels)	0.95	0.86
RMSE after deleting outliers (pixels)	0.77	0.54

Table 1. The result of different matching methods

4. CONCLUSIONS AND DISCUSSION

The experimental result shows that the proposed algorithm which combines the feature-based with area-based matching methods can not only register two multi-source images successfully, but also improve the accuracy and precision comparing to the feature-based matching method only. It is explained that segmenting images and adjusting image radiometric parameters are effective.

The dataset of the experiment is in a flat area, so more areas with height difference will be tested, using the proposed algorithm. It will also be tested for more kinds of remote sensing images, such as Quickbird and ERS2, in order to achieve the aim of more applications.

REFERENCES

- Bentoutou, Y., N. Taleb, K. Kpalma, and J. Ronsin, 2005. An automatic image registration for applications in remote sensing. *IEEE Transaction on Geoscience and Remote Sensing*, 43(9), pp. 2127-2137.
- Canny, J., 1986. A computational approach to edge detection. *IEEE Transactions on Pattern Analysis and Machine Intelligence*, 8(6), pp. 679-698.
- Chen, F., Wang, C., and Zhang, H., 2007. Automatic matching of high-resolution SAR images. *International Journal of Remote Sensing*, 28(16), pp. 3665-3678.
- Dai, X., 1999. A feature-based image registration algorithm using improved chain-code representation combined with invariant moments. *IEEE Transactions on Geoscience and Remote Sensing*, 37(5), pp. 2351-2362.
- Dare, P. and Dowman, I., 2001. An improved model for automatic feature-based registration of SAR and SPOT images. *ISPRS Journal of Photogrammetry and Remote Sensing*, 56(1), pp. 13-28.
- Goshtasby, A., 1988. Registration of images with geometric distortions. *IEEE Transactions on Geoscience and Remote Sensing*, 26(1), pp. 60-64.
- Hong, T. D. and R. A. Schowengerdt, 2005. A robust technique for precise registration of radar and optical satellite images. *Photogrammetric Engineering & Remote Sensing*, 71(5), pp. 585-593.
- Newton, W., C. Gurney, D. Sloggett, and I. Dowman, 1994. An approach to the automated identification of forests and forest change in remotely sensed images. *International Archives of Photogrammetry and Remote Sensing*. 30(3), pp. 607-614.
- Tsai, D. M., 1995. A fast thresholding selection procedure for multimodel and unimodel histograms. *Pattern Recognition Letters*, 16(6), pp. 653-666.
- Zitova, B. and Flusser, J., 2003. Image registration methods: a survey. *Image and Vision Computing*, 21(11), pp. 977-1000.